A Three-Dimensional Mathematical Model for Groundwater Level Variations in a Two-Layered Medium

Sherzod Daliev
Kattakurgan Branch of Samarkand State University, Uzbekistan
daliyevsherzod87@gmail.com (corresponding author)

Sherzod Urakov
Kattakurgan Branch of Samarkand State University, Uzbekistan
usherzod78@gmail.com

Ulugbek Elmurodov
Kattakurgan Branch of Samarkand State University, Uzbekistan
elmurodovulugbek32@gmail.com

Oxun Xaitov
Kattakurgan Branch of Samarkand State University, Uzbekistan
xaitovoxunjon1995@gmail.com

Maftuna Abbasova
Kattakurgan Branch of Samarkand State University, Uzbekistan
maftuna08011993@gmail.com

Received: 10 May 2025 | Revised: 30 June 2025, 15 July 2025, and 4 August 2025 | Accepted: 9 August 2025

 DOI: https://doi.org/10.48084/etasr.11979

ABSTRACT

Studying the hydrodynamic regime of groundwater, particularly the formation of new freshwater reserves and monitoring their quantitative and qualitative indicators, holds significant scientific and practical importance. In this research, the main causes of groundwater level variations in two-layer media were analyzed, including precipitation and evaporation, water extraction and recharge sources, geological structure and interlayer permeability characteristics, hydraulic gradient, flow directions, water infiltration due to irrigation, filtration coefficient, porosity, layer thickness, drainage, and artesian wells. To accurately model the variations in the water levels of unconfined and confined aquifers, a mathematical model was developed that accounts for the physical-geological and hydrogeological parameters of the study area. The problem was described through mathematical and numerical modeling of geofiltration and geomigration processes. The model is represented by nonlinear differential equations, which do not have an analytical solution due to the presence of free variables. Therefore, a fully stable numerical solution scheme based on high-precision approximation was proposed. The solutions were obtained using iterative calculations and forward-backward substitution methods. The research also considered parameters, such as soil density, effective porosity, and third-order open boundary conditions. As a result, the model provides reliable forecasts for identifying groundwater movement and quality changes. This method offers practical Psolutions that can be applied in water resource management and planning.

Keywords-groundwater hydrodynamics; groundwater modeling; numerical simulation; geofiltration

I. INTRODUCTION

The artificial recharge of riverbed lenses is an effective measure for increasing the freshwater reserves and improving the groundwater quality. However, in the downstream sections of the rivers in Central Asia, freshwater inflow is now concentrated mainly during flood periods due to changes in the water management practices. As a result, the reserves of freshwater lenses are declining, and the extracted water often exceeds permissible limits of salinity and hardness. This makes

the artificial formation and replenishment of riverbed lenses an urgent scientific and practical task.

The procedure of the artificial recharge involves hydrogeological, hydrological, and technical measures aimed at supplementing riverbed aquifers, stabilizing their flow, and improving groundwater quality. It is implemented by introducing freshwater into aquifers adjacent to river channels, typically in areas with reliable flow and increases both the storage capacity of lenses and the overall water reserves.

The scientific analysis of the water structure indicates that there are two main approaches to modeling this process: homogeneous and heterogeneous models. This distinction becomes especially evident when describing the interaction of nonelectrolytes with aqueous solutions. Research confirms that only heterogeneous models, particularly the two-structure model, can accurately explain the mutual solubility process of non-polar gases in water. According to this model, each structural component possesses specific physicochemical properties and occupies a definite volume in space.

To analyze the movement processes of groundwater components within the pores and fractures of rocks, it is necessary to thoroughly study the migration processes of subsurface fractured-porous fluids. In this context, it is essential to account for the physicochemical transformations that occur as groundwater interacts with geological formations. The hydrodynamic principles of groundwater migration, based on the concepts of heat and mass transfer, serve as a fundamental basis for developing quantitative methods to assess the qualitative composition of water during flow processes. These principles enable the creation of methodological tools necessary for scientifically justifying and effectively managing the mechanisms of artificial recharge of riverbed lenses.

The Artificial Intelligence (AI) and Machine Learning (ML) approaches have gained prominence in forecasting groundwater level fluctuations. These methods have demonstrated high predictive accuracy and can enhance the traditional deterministic modeling techniques by increasing precision and reducing computational time [1, 2]. Despite these advancements, the present study focuses on developing a three-dimensional deterministic model, with ML techniques employed only for validation and comparative analysis.

Numerical and deterministic modeling has been widely applied to groundwater flow and salinization processes, including MODFLOW and MT3DMS simulations, as well as studies on urban, coastal, and agricultural areas [3-5]. These approaches provide a framework for predicting salinization risks, climate impacts, and anthropogenic influences on groundwater quality [6-8]. Research on artificial recharge techniques, long-term salinization prediction, and saltwater intrusion further demonstrates the practical application of modeling for water resource management [9-11].

Additional studies have examined the impact of irrigation, fertilizers, and climate change on groundwater salinity, highlighting the importance of integrated modeling in resource management and salinity mitigation [12-14]. Investigations into analytical and numerical methods, remote sensing, and geophysical monitoring have provided further validation and operational insights for managing groundwater quality [15-18]. Modeling and simulation continue to be essential tools due to their practical applicability and ability to support complex analyses [19-22].

Based on this body of research, the development of an improved three-dimensional mathematical model expressed through nonlinear differential equations is both scientifically and practically necessary. The proposed model will describe groundwater level variations in a two-layer subsurface system adjacent to riverbeds and will provide an integrated framework to evaluate climate impacts, hydrogeological conditions, anthropogenic pressures, and artificial recharge effects. It will, thus, support effective strategies for groundwater resource management.

II. PROBLEM STATEMENT AND MATHEMATICAL MODEL

The study of groundwater level dynamics is a key issue in hydrogeology, water resource management, and environmental monitoring. In a two-layered subsurface medium, fluctuations in groundwater levels arise under the combined influence of natural and anthropogenic factors, including precipitation and evaporation, water abstraction and recharge, geological structure and permeability, as well as the regional hydraulic gradient and flow direction.

To analyze these processes, mathematical and numerical modeling of geofiltration is employed, providing tools for effective monitoring and practical recommendations. The governing problem can be formulated as a system of nonlinear differential equations (1), which represent a three-dimensional mathematical model describing groundwater level variations in two-layered media [28-30]:

$$\left.\begin{aligned}
&\mu_1 n_0 \frac{\partial h}{\partial t} = \frac{\partial}{\partial x}(k_1 h \frac{\partial h}{\partial x}) + \frac{\partial}{\partial y}(k_1 h \frac{\partial h}{\partial y}) + \\
&+ \frac{\partial}{\partial z}(k_1 h \frac{\partial h}{\partial z}) + k_1 \frac{H-h}{m} + f - \omega, \\
&\mu_2 \frac{\partial H}{\partial t} = \frac{\partial}{\partial x}(k_2 H \frac{\partial H}{\partial x}) + \frac{\partial}{\partial y}(k_2 H \frac{\partial H}{\partial y}) + \\
&+ \frac{\partial}{\partial z}(k_2 H \frac{\partial H}{\partial z}) + k_2 \frac{h-H}{m} - \eta Q
\end{aligned}\right\} \quad (1)$$

where $h(x,y,z,t)$, $H(x,y,z,t)$ denote the levels of unconfined and confined groundwater, respectively, μ_1, μ_2 are the coefficients of water loss, k_1, k_2 are the filtration coefficients of the upper and lower formations, f is the external source, n_0 is the porosity, ω is the evaporation, m is the thickness of the separating layer, Q is the debit, and η is the coefficient for converting the model into a dimensional form (the mass balance coefficient).

The system of equations (1) is solved under the following initial (2) and boundary conditions (3-8):

$$h(x, y, z, t_0) = h_0,\ H(x, y, z, t_0) = H_0,\ t = t_0 \quad (2)$$

$$\mu_1 n_0 h \frac{\partial h}{\partial x}\bigg|_{x=0} = -(h-h_0), \mu_1 n_0 h \frac{\partial h}{\partial x}\bigg|_{x=L_x} = (h-h_0) \quad (3)$$

$$\mu_1 n_0 h \frac{\partial h}{\partial y}\bigg|_{y=0} = -(h-h_0), \mu_1 n_0 h \frac{\partial h}{\partial y}\bigg|_{y=L_y} = (h-h_0) \quad (4)$$

$$\mu_1 n_0\, m \frac{\partial h}{\partial z}\bigg|_{z=0} = -(h-h_0), \mu_1 n_0\, m \frac{\partial h}{\partial z}\bigg|_{z=L_z} = (h-h_0) \quad (5)$$

$$\mu_2 H \frac{\partial H}{\partial x}\bigg|_{x=0} = -(H-H_0), \mu_2 H \frac{\partial H}{\partial x}\bigg|_{x=L_x} = (H-H_0) \quad (6)$$

$$\mu_2 H \frac{\partial H}{\partial y}\bigg|_{y=0} = -(H-H_0), \mu_2 H \frac{\partial H}{\partial y}\bigg|_{y=L_y} = (H-H_0) \quad (7)$$

$$\mu_2\, m \frac{\partial H}{\partial z}\bigg|_{z=0} = -(H-H_0), \mu_2\, m \frac{\partial H}{\partial z}\bigg|_{z=L_z} = (H-H_0) \quad (8)$$

where h_0 and H_0 are the initial levels of phreatic and confined waters and L_x, L_y, L_z are the spatial coordinates along the Cartesian axes corresponding to the principal directions of the three-dimensional Euclidean space ($L_x = L_y = L_z = L$).

This framework has practical applications in Uzbekistan, particularly in the Amu Darya and Syr Darya basins, where irrigation-induced rises in groundwater levels contribute to salinization. The model quantifies the impact of infiltration (μ_1, μ_2) and evaporation (ω) associated with irrigation practices. In urban areas, such as Tashkent, groundwater rise threatens construction stability by undermining foundations. Here, the model assists in predicting groundwater movement and optimizing drainage systems for urban planning. In oil and gas fields, the interaction of unconfined and confined water levels $h(x,y,z,t)$, $H(x,y,z,t)$, filtration coefficients (k_1, k_2), and external sources (f) influences hydrocarbon extraction. Modeling these processes enables improved resource management and exploitation efficiency.

The model incorporates several physical parameters essential for capturing the hydrogeological processes. The filtration coefficients (k_1, k_2) describe soil permeability, which varies across regions. For example, sandy soils in Tashkent enhance filtration, while clay layers in Bukhara limit it. Porosity (n_0) reflects the capacity of soils and rocks to retain water. Its value is high in sandy desert formations and low in mountainous terrains. Evaporation (ω) accounts for climatic effects. In Karakalpakstan, high temperatures and arid conditions lead to significant groundwater losses. The thickness (m) of the separating layer influences storage potential, as thinner layers in regions like Bukhara may limit reserves. Debit (Q) captures the discharge and infiltration processes, which are especially relevant in Surkhandarya, where drainage systems actively regulate groundwater.

Overall, the model provides a comprehensive mathematical framework for analyzing groundwater and pressurized water dynamics, supporting monitoring in irrigated zones, forecasting for urban infrastructure, and assessing layer interactions in hydrocarbon fields. The governing equations and boundary conditions account for critical processes, such as evaporation, infiltration, filtration, porosity effects, external influences, drainage, and artesian well impacts, ensuring that the model realistically reflects geological environments, enabling its application in groundwater forecasting, risk assessment, water conservation, and sustainable management strategies.

III. SOLUTION METHOD

To solve the problem expressed by (1-8), the following dimensionless variables are introduced [23-24]:

$$\left.\begin{aligned} &h^* = \frac{h}{h_0}, H^* = \frac{H}{L}, x^* = \frac{x}{L}, y^* = \frac{y}{L}, z^* = \frac{z}{L}, \\ &k_1^* = \frac{k_1}{(k_1)_0}, k_2^* = \frac{k_2}{(k_2)_0}, m^* = \frac{m}{m_0}, \tau = \frac{(k_1)_0 h_0}{\mu_1 n_0 L^2} t, \\ &Q^* = \frac{Q}{Q_0} \end{aligned}\right\} \quad (9)$$

Thus, the initial problem takes the following form:

$$\left.\begin{aligned} &\frac{\partial h^*}{\partial \tau} = \frac{\partial}{\partial x^*}(k_1^* h^* \frac{\partial h^*}{\partial x^*}) + \frac{\partial}{\partial y^*}(k_1^* h^* \frac{\partial h^*}{\partial y^*}) + \\ &+ \frac{\partial}{\partial z^*}(k_1^* h^* \frac{\partial h^*}{\partial z^*}) + \xi k_1^* \frac{H^* - \xi_1 h^*}{m^*} + \xi_2 (f - \omega), \\ &\frac{\partial H^*}{\partial t} = \varphi \frac{\partial}{\partial x^*}(k_2^* H^* \frac{\partial H^*}{\partial x^*}) + \varphi \frac{\partial}{\partial y^*}(k_2^* H^* \frac{\partial H^*}{\partial y^*}) + \\ &+ \varphi \frac{\partial}{\partial z^*}(k_2^* H^* \frac{\partial H^*}{\partial z^*}) + \varphi_1 k_2^* \frac{\xi_1 h^* - H^*}{m^*} - \varphi_2 \eta Q^* \end{aligned}\right\} \quad (10)$$

where $\xi, \xi_1, \xi_2, \varphi, \varphi_1, \varphi_2$ are defined by:

$$\left.\begin{aligned} &\xi = \frac{H_0 L^2}{m_0 h_0},\ \xi_1 = \frac{h_0}{H_0},\ \xi_2 = \frac{L^2}{(k_1)_0 h_0^2}, \\ &\varphi = \frac{\mu_1 n_0 H_0 (k_2)_0 L^2}{\mu_2 (k_1)_0 h_0}, \varphi_1 = \frac{\varphi L^2}{m_0 H_0}, \\ &\varphi_2 = \frac{\mu_1 n_0 L^2 \eta Q_0}{\mu_2 (k_1)_0 h_0 H_0} \end{aligned}\right\} \quad (11)$$

with the initial and boundary conditions expressed as:

$$h\big|_{\tau=0} = h_0, H\big|_{\tau=0} = H_0 \quad (12)$$

$$\left.\begin{aligned} &\frac{\mu_1 n_0 h_0^2}{L} h^* \frac{\partial h^*}{\partial x^*}\bigg|_{x^*=0} = -h_0 (h^* - 1), \\ &\frac{\mu_1 n_0 h_0^2}{L} h^* \frac{\partial h^*}{\partial x^*}\bigg|_{x^*=1} = h_0 (h^* - 1) \end{aligned}\right\} \quad (13)$$

$$\left.\begin{aligned} &\frac{\mu_1 n_0 h_0^2}{L} h^* \frac{\partial h^*}{\partial y^*}\bigg|_{y^*=0} = -h_0 (h^* - 1), \\ &\frac{\mu_1 n_0 h_0^2}{L} h^* \frac{\partial h^*}{\partial y^*}\bigg|_{y^*=1} = h_0 (h^* - 1) \end{aligned}\right\} \quad (14)$$

$$\left.\begin{aligned}\frac{\mu_1 n_0 h_0 m_0}{L} m^* \left.\frac{\partial h^*}{\partial z^*}\right|_{z^*=0} &= -h_0(h^*-1),\\ \frac{\mu_1 n_0 h_0 m_0}{L} m^* \left.\frac{\partial h^*}{\partial z^*}\right|_{z^*=1} &= h_0(h^*-1)\end{aligned}\right\} \quad (15)$$

$$\left.\begin{aligned}\frac{\mu_2 H_0^2}{L} H^* \left.\frac{\partial H^*}{\partial x^*}\right|_{x^*=0} &= -H_0(H^*-1),\\ \frac{\mu_2 H_0^2}{L} H^* \left.\frac{\partial H^*}{\partial x^*}\right|_{x^*=1} &= H_0(H^*-1)\end{aligned}\right\} \quad (16)$$

$$\left.\begin{aligned}\frac{\mu_2 H_0^2}{L} H^* \left.\frac{\partial H^*}{\partial y^*}\right|_{y^*=0} &= -H_0(H^*-1),\\ \frac{\mu_2 H_0^2}{L} H^* \left.\frac{\partial H^*}{\partial y^*}\right|_{y^*=1} &= H_0(H^*-1)\end{aligned}\right\} \quad (17)$$

$$\left.\begin{aligned}\frac{\mu_2 m_0 H_0}{L} m^* \left.\frac{\partial H^*}{\partial z^*}\right|_{z^*=0} &= -H_0(H^*-1),\\ \frac{\mu_2 m_0 H_0}{L} m^* \left.\frac{\partial H^*}{\partial z^*}\right|_{z^*=1} &= H_0(H^*-1)\end{aligned}\right\} \quad (18)$$

Using the dimensional variables (9), equation (10) takes the following form:

$$\left.\begin{aligned}&\frac{\partial h}{\partial \tau} = \frac{\partial}{\partial x}(k_1 h \frac{\partial h}{\partial x}) + \frac{\partial}{\partial y}(k_1 h \frac{\partial h}{\partial y}) +\\ &+\frac{\partial}{\partial z}(k_1 h \frac{\partial h}{\partial z}) + \xi k_1 \frac{H-\xi_1 h}{m} + \xi_2 (f-\omega),\\ &\frac{\partial H}{\partial \tau} = \varphi \frac{\partial}{\partial x}(k_2 H \frac{\partial H}{\partial x}) + \varphi \frac{\partial}{\partial y}(k_2 H \frac{\partial H}{\partial y}) +\\ &+\varphi \frac{\partial}{\partial z}(k_2 H \frac{\partial H}{\partial z}) + \varphi_1 k_2 \frac{\xi_1 h - H}{m} - \varphi_2 \eta Q\end{aligned}\right\} \quad (19)$$

with the initial and boundary conditions expressed as:

$$h\big|_{\tau=0} = h_0, H\big|_{\tau=0} = H_0 \quad (20)$$

$$\left.\begin{aligned}\frac{\mu_1 n_0 h_0^2}{L} h \left.\frac{\partial h}{\partial x}\right|_{x=0} &= -h_0(h-1),\\ \frac{\mu_1 n_0 h_0^2}{L} h \left.\frac{\partial h}{\partial x}\right|_{x=1} &= h_0(h-1)\end{aligned}\right\} \quad (21)$$

$$\left.\begin{aligned}\frac{\mu_1 n_0 h_0^2}{L} h \left.\frac{\partial h}{\partial y}\right|_{y=0} &= -h_0(h-1),\\ \frac{\mu_1 n_0 h_0^2}{L} h \left.\frac{\partial h}{\partial y}\right|_{y=1} &= h_0(h-1)\end{aligned}\right\} \quad (22)$$

$$\left.\begin{aligned}\frac{\mu_1 n_0 h_0 m_0}{L} m \left.\frac{\partial h}{\partial z}\right|_{z=0} &= -h_0(h-1),\\ \frac{\mu_1 n_0 h_0 m_0}{L} m \left.\frac{\partial h}{\partial z}\right|_{z=1} &= h_0(h-1)\end{aligned}\right\} \quad (23)$$

$$\left.\begin{aligned}\frac{\mu_2 H_0^2}{L} H \left.\frac{\partial H}{\partial x}\right|_{x=0} &= -H_0(H-1),\\ \frac{\mu_2 H_0^2}{L} H \left.\frac{\partial H}{\partial x}\right|_{x=1} &= H_0(H-1)\end{aligned}\right\} \quad (24)$$

$$\left.\begin{aligned}\frac{\mu_2 H_0^2}{L} H \left.\frac{\partial H}{\partial y}\right|_{y=0} &= -H_0(H-1),\\ \frac{\mu_2 H_0^2}{L} H \left.\frac{\partial H}{\partial y}\right|_{y=1} &= H_0(H-1)\end{aligned}\right\} \quad (25)$$

$$\left.\begin{aligned}\frac{\mu_2 m_0 H_0}{L} m \left.\frac{\partial H}{\partial z}\right|_{z=0} &= -H_0(H-1),\\ \frac{\mu_2 m_0 H_0}{L} m \left.\frac{\partial H}{\partial z}\right|_{z=1} &= H_0(H-1)\end{aligned}\right\} \quad (26)$$

Since this problem represents a system of nonlinear partial differential equations, an analytical solution is not feasible. Therefore, the finite difference method is applied [24-25]. A computational grid is introduced to approximate the solution domain *D*, which is defined as the spatio-temporal region where the governing differential equations are solved. Within this domain, all initial and boundary conditions are specified, enabling the evaluation of parameters, such as pressure, concentration, and velocity, across space and time. The domain is expressed as:

$$D = \left\{ \begin{aligned}&(x, y, z, t) \in R^4 \,\big|\, 0 \le x \le L,\ 0 \le y \le L,\\ &0 \le z \le L,\ 0 \le t \le N\end{aligned} \right\} \quad (27)$$

where *x, y, z* are the spatial coordinates, *t* denotes time, and *L, N* are the respective upper bounds of the domain in space and time.

This continuous domain is discretized into a grid:

$$\omega_{\Delta x,\Delta y,\Delta z,\Delta \tau} = \left(x_i, y_j, z_k, t_n\right) = \left(i\Delta x, j\Delta y, k\Delta z, n\Delta\tau\right) \quad (28)$$

with $i = 0,1,2,...I$, $j = 0,1,2,...J$, $k = 0,1,2,...K$, $n = 0,1,2,...,N$.

Since the system is nonlinear with respect to the surface functions, it is reformulated into a quasi-linear approximation. Using a grid with $n+\frac{1}{3}$ layers in time and $\omega_{\Delta x,\Delta y,\Delta z,\Delta \tau}$ points over time, the explicit finite difference scheme is applied and the nonlinear term is linearized using:

$$h^2 \approx 2\tilde{h}h - \tilde{h}^2 \quad (29)$$

This leads to the quasilinear system:

$$a_{i,j,k}h_{i-1,j,k}^{n+\frac{1}{3}} - b_{i,j,k}h_{i,j,k}^{n+\frac{1}{3}} + c_{i,j,k}h_{i+1,j,k}^{n+\frac{1}{3}} = -d_{i,j,k}^{n} \quad (30)$$

$$\overline{a}_{i,j,k}H_{i-1,j,k}^{n+\frac{1}{3}} - \overline{b}_{i,j,k}H_{i,j,k}^{n+\frac{1}{3}} + \overline{c}_{i,j,k}H_{i+1,j,k}^{n+\frac{1}{3}} = -\overline{d}_{i,j,k}^{n} \quad (31)$$

with the boundary conditions being approximated with second-order accuracy at:

$$\left.\begin{aligned}\frac{\mu_1 n_0 h_0^2}{4\Delta xL}\left(h_{0,j,k}^{n+\frac{1}{3}} - 4h_{1,j,k}^{n+\frac{1}{3}} + 3h_{2,j,k}^{n+\frac{1}{3}}\right) &= -h_0(h_{1,j,k}^{n+\frac{1}{3}} - 1)\\ \frac{\mu_0 n_0 h_0^2}{4\Delta xL}\left(-3h_{I-1,j,k}^{n+\frac{1}{3}} + 4h_{I,j,k}^{n+\frac{1}{3}} - h_{I+1,j,k}^{n+\frac{1}{3}}\right) &= h_0(h_{I,j,k}^{n+\frac{1}{3}} - 1)\end{aligned}\right\} \quad (32)$$

$$\left.\begin{aligned}\frac{\mu_1 n_0 h_0^2}{4\Delta yL}\left(h_{i,0,k}^{n+\frac{2}{3}} - 4h_{i,1,k}^{n+\frac{2}{3}} + 3h_{i,2,k}^{n+\frac{2}{3}}\right) &= -h_0(h_{i,1,k}^{n+\frac{2}{3}} - 1)\\ \frac{\mu_0 n_0 h_0^2}{4\Delta yL}\left(-3h_{i,J-1,k}^{n+\frac{2}{3}} + 4h_{i,J,k}^{n+\frac{2}{3}} - h_{i,J+1,k}^{n+\frac{2}{3}}\right) &= h_0(h_{i,J,k}^{n+\frac{2}{3}} - 1)\end{aligned}\right\} \quad (33)$$

$$\left.\begin{aligned}&\frac{\mu_1 n_0 h_0 m_0}{2\Delta zL} m_{i,j,1}\left(h_{i,j,0}^{n+1} - 4h_{i,j,1}^{n+1} + 3h_{i,j,2}^{n+1}\right) =\\ &= -h_0(h_{i,j,1}^{n+1} - 1)\\ &\frac{\mu_1 n_0 h_0 m_0}{2\Delta zL} m_{i,j,K}\left(-3h_{i,j,K-1}^{n+1} + 4h_{i,j,K}^{n+1} - h_{i,j,K+1}^{n+1}\right) =\\ &= h_0(h_{i,j,K}^{n+1} - 1)\end{aligned}\right\} \quad (34)$$

$$\left.\begin{aligned}&\frac{\mu_2 H_0^2}{4\Delta xL}\left(H_{0,j,k}^{n+\frac{1}{3}} - 4H_{1,j,k}^{n+\frac{1}{3}} + 3H_{2,j,k}^{n+\frac{1}{3}}\right) =\\ &= -H_0(H_{1,j,k}^{n+\frac{1}{3}} - 1)\\ &\frac{\mu_2 H_0^2}{4\Delta xL}\left(-3H_{I-1,j,k}^{n+\frac{1}{3}} + 4H_{I,j,k}^{n+\frac{1}{3}} - H_{I+1,j,k}^{n+\frac{1}{3}}\right) =\\ &= H_0(H_{I,j,k}^{n+\frac{1}{3}} - 1)\end{aligned}\right\} \quad (35)$$

$$\left.\begin{aligned}&\frac{\mu_2 H_0^2}{4\Delta yL}\left(H_{i,0,k}^{n+\frac{2}{3}} - 4H_{i,1,k}^{n+\frac{2}{3}} + 3H_{i,2,k}^{n+\frac{2}{3}}\right) =\\ &= -H_0(H_{i,1,k}^{n+\frac{2}{3}} - 1)\\ &\frac{\mu_2 H_0^2}{4\Delta yL}\left(-3H_{i,J-1,k}^{n+\frac{2}{3}} + 4H_{i,J,k}^{n+\frac{2}{3}} - H_{i,J+1,k}^{n+\frac{2}{3}}\right) =\\ &= H_0(H_{i,J,k}^{n+\frac{2}{3}} - 1)\end{aligned}\right\} \quad (36)$$

$$\left.\begin{aligned}&\frac{\mu_2 m_0 H_0}{2\Delta zL} m_{i,j,1}\left(H_{i,j,0}^{n+1} - 4H_{i,j,1}^{n+1} + 3H_{i,j,2}^{n+1}\right) =\\ &= -H_0(H_{i,j,1}^{n+1} - 1)\\ &\frac{\mu_2 m_0 H_0}{2\Delta zL} m_{i,j,K}\left(-3H_{i,j,K-1}^{n+1} + 4H_{i,j,K}^{n+1} - H_{i,j,K+1}^{n+1}\right) =\\ &= H_0(H_{i,j,K}^{n+1} - 1)\end{aligned}\right\} \quad (37)$$

The algebraic system of (30, 31) is solved using the sweep method and the following recurrence relations:

$$\left.\begin{aligned}h_{i,j,k}^{n+\frac{1}{3}} &= \alpha_{i+1,j,k}h_{i+1,j,k}^{n+\frac{1}{3}} + \beta_{i+1,j,k}\\ H_{i,j,k}^{n+\frac{1}{3}} &= \overline{\alpha}_{i+1,j,k}H_{i+1,j,k}^{n+\frac{1}{3}} + \overline{\beta}_{i+1,j,k}\end{aligned}\right\} \quad (38)$$

where $\alpha_{i+1,j,k}, \beta_{i+1,j,k}, \overline{\alpha}_{i+1,j,k}, \overline{\beta}_{i+1,j,k}$ are the sweep coefficients.

Replacing i with i-1, the recurrence equations (38) take the next form:

$$\left.\begin{aligned}h_{i-1,j,k}^{n+\frac{1}{3}} &= \alpha_{i,j,k}h_{i,j,k}^{n+\frac{1}{3}} + \beta_{i,j,k}\\ H_{i-1,j,k}^{n+\frac{1}{3}} &= \overline{\alpha}_{i,j,k}H_{i,j,k}^{n+\frac{1}{3}} + \overline{\beta}_{i,j,k}\end{aligned}\right\} \quad (39)$$

Assuming i=1, the system of tridiagonal linear algebraic equations (30, 31), along with the recurrence equations (39), leads to:

$$\left.\begin{aligned}h_{2,j,k}^{n+\frac{1}{3}} &= -\frac{a_{1,j,k}}{c_{1,j,k}}h_{0,j,k}^{n+\frac{1}{3}} + \frac{b_{1,j,k}}{c_{1,j,k}}h_{1,j,k}^{n+\frac{1}{3}} - \frac{d_{1,j,k}^{n}}{c_{1,j,k}}\\ H_{2,j,k}^{n+\frac{1}{3}} &= -\frac{\overline{a}_{1,j,k}}{\overline{c}_{1,j,k}}H_{0,j,k}^{n+\frac{1}{3}} + \frac{\overline{b}_{1,j,k}}{\overline{c}_{1,j,k}}H_{1,j,k}^{n+\frac{1}{3}} - \frac{\overline{d}_{1,j,k}^{n}}{\overline{c}_{1,j,k}}\end{aligned}\right\} \quad (40)$$

$$\left.\begin{aligned}h_{0,j,k}^{n+\frac{1}{3}} &= \alpha_{1,j,k}h_{1,j,k}^{n+\frac{1}{3}} + \beta_{1,j,k}\\ H_{0,j,k}^{n+\frac{1}{3}} &= \overline{\alpha}_{1,j,k}H_{1,j,k}^{n+\frac{1}{3}} + \overline{\beta}_{1,j,k}\end{aligned}\right\} \quad (41)$$

By simplifying the boundary conditions, we obtain:

$$\left.\begin{aligned}h_{2,j,k}^{n+\frac{1}{3}} &= -\frac{1}{3}h_{0,j,k}^{n+\frac{1}{3}} + \left(\frac{4}{3} - \frac{4\Delta xL}{3\mu_1 n_0 h_0}\right)h_{1,j,k}^{n+\frac{1}{3}} + \frac{4\Delta xL}{3\mu_1 n_0 h_0},\\ H_{2,j,k}^{n+\frac{1}{3}} &= -\frac{1}{3}H_{0,j,k}^{n+\frac{1}{3}} + \left(\frac{4}{3} - \frac{4\Delta xL}{3\mu_2 H_0}\right)H_{1,j,k}^{n+\frac{1}{3}} + \frac{4\Delta xL}{3\mu_2 H_0}\end{aligned}\right\} \quad (42)$$

By comparing (40) and (42) the values of $h_{0,j,k}^{n+\frac{1}{3}}$ and $H_{0,j,k}^{n+\frac{1}{3}}$ are determined:

$$\left.\begin{aligned}h_{0,j,k}^{n+\frac{1}{3}} &= \frac{3\mu_1 n_0 h_0 b_{1,j,k} - 4c_{1,j,k}\mu_1 n_0 h_0 + 4\Delta xLc_{1,j,k}}{\mu_1 n_0 h_0(3a_{1,j,k} - c_{1,j,k})}h_{1,j,k}^{n+\frac{1}{3}} -\\ &- \frac{3d_{1,j,k}^{n}\mu_1 n_0 h_0 + 4\Delta xLc_{1,j,k}}{\mu_1 n_0 h_0(3a_{1,j,k} - c_{1,j,k})},\\ H_{0,j,k}^{n+\frac{1}{3}} &= \frac{3\overline{b}_{1,j,k}\mu_2 H_0 - 4\overline{c}_{1,j,k}\mu_2 H_0 - 4\Delta xL\overline{c}_{1,j,k}}{\mu_2 H_0(3\overline{a}_{1,j,k} - \overline{c}_{1,j,k})}H_{1,j,k}^{n+\frac{1}{3}} -\\ &- \frac{3\overline{d}_{1,j,k}^{n}\mu_2 H_0 + 4\Delta xL\overline{c}_{1,j,k}}{\mu_2 H_0(3\overline{a}_{1,j,k} - \overline{c}_{1,j,k})}\end{aligned}\right\} \quad (43)$$

By comparing (41) and (43) the initial values of the coefficients $\alpha_{i+1,j,k}, \beta_{i+1,j,k}, \overline{\alpha}_{i+1,j,k}, \overline{\beta}_{i+1,j,k}$ are determined:

$$\left.\begin{aligned}
\alpha_{1,j,k} &= \frac{3\mu_1 n_0 h_0 b_{1,j,k} - 4c_{1,j,k}\mu_1 n_0 h_0 + 4\Delta x L c_{1,j,k}}{\mu_1 n_0 h_0 (3a_{1,j,k} - c_{1,j,k})}, \\
\beta_{1,j,k} &= -\frac{3d^n_{1,j,k}\mu_1 n_0 h_0 + 4\Delta x L c_{1,j,k}}{\mu_1 n_0 h_0 (3a_{1,j,k} - c_{1,j,k})}, \\
\bar{\alpha}_{1,j,k} &= \frac{3\bar{b}_{1,j,k}\mu_2 H_0 - 4\bar{c}_{1,j,k}\mu_2 H_0 - 4\Delta x L \bar{c}_{1,j,k}}{\mu_2 H_0 (3\bar{a}_{1,j,k} - \bar{c}_{1,j,k})}, \\
\bar{\beta}_{1,j,k} &= -\frac{3\bar{d}^n_{1,j,k}\mu_2 H_0 + 4\Delta x L \bar{c}_{1,j,k}}{\mu_2 H_0 (3\bar{a}_{1,j,k} - \bar{c}_{1,j,k})}
\end{aligned}\right\} \quad (44)$$

Assuming $i=I$ in the tridiagonal linear algebraic system of (30, 31), as well as in the recurrent equations (38), we get:

$$\left.\begin{aligned}
h^{n+\frac{1}{3}}_{I+1,j,k} &= \frac{b_{I,j,k}}{c_{I,j,k}} h^{n+\frac{1}{3}}_{I,j,k} - \frac{a_{I,j,k}}{c_{I,j,k}} h^{n+\frac{1}{3}}_{I-1,j,k} - \frac{d^n_{I,j,k}}{c_{I,j,k}}, \\
H^{n+\frac{1}{3}}_{I+1,j,k} &= \frac{\bar{b}_{I,j,k}}{\bar{c}_{I,j,k}} H^{n+\frac{1}{3}}_{I,j,k} - \frac{\bar{a}_{I,j,k}}{\bar{c}_{I,j,k}} H^{n+\frac{1}{3}}_{I-1,j,k} - \frac{\bar{d}^n_{I,j,k}}{\bar{c}_{I,j,k}},
\end{aligned}\right\} \quad (45)$$

$$\left.\begin{aligned}
h^{n+\frac{1}{3}}_{I-1,j,k} &= \alpha_{I,j,k} h^{n+\frac{1}{3}}_{I,j,k} + \beta_{I,j,k}, \\
H^{n+\frac{1}{3}}_{I-1,j,k} &= \bar{\alpha}_{I,j,k} H^{n+\frac{1}{3}}_{I,j,k} + \bar{\beta}_{I,j,k}
\end{aligned}\right\} \quad (46)$$

Simplifying the boundary conditions (32) and (35), we obtain:

$$\left.\begin{aligned}
h^{n+\frac{1}{3}}_{I+1,j,k} &= \left(4 - \frac{4\Delta x L}{\mu_0 n_0 h_0}\right) h^{n+\frac{1}{3}}_{I,j,k} - 3h^{n+\frac{1}{3}}_{I-1,j,k} + \frac{4\Delta x L}{\mu_0 n_0 h_0} \\
H^{n+\frac{1}{3}}_{I+1,j,k} &= \left(4 - \frac{4\Delta x L}{\mu_2 H_0}\right) H^{n+\frac{1}{3}}_{I,j,k} - 3H^{n+\frac{1}{3}}_{I-1,j,k} + \frac{4\Delta x L}{\mu_2 H_0}
\end{aligned}\right\} \quad (47)$$

Comparing (45) with (46) the values for $h^{n+\frac{1}{3}}_{I-1,j,k}$ and $H^{n+\frac{1}{3}}_{I-1,j,k}$ are determined:

$$\left.\begin{aligned}
h^{n+\frac{1}{3}}_{I-1,j,k} &= \frac{4\mu_0 n_0 h_0 c_{I,j,k} - 4\Delta x L c_{I,j,k} - b_{I,j,k}\mu_0 n_0 h_0}{\mu_0 n_0 h_0 (3c_{I,j,k} - a_{I,j,k})} h^{n+\frac{1}{3}}_{I,j,k} + \\
&+ \frac{\mu_0 n_0 h_0 d^n_{I,j,k} + 4\Delta x L c_{I,j,k}}{\mu_0 n_0 h_0 (3c_{I,j,k} - a_{I,j,k})}, \\
H^{n+\frac{1}{3}}_{I-1,j,k} &= \frac{4\bar{c}_{I,j,k} - 4\Delta x L - \mu_2 H_0 \bar{b}_{I,j,k}}{\mu_2 H_0 (3\bar{c}_{I,j,k} - \bar{a}_{I,j,k})} H^{n+\frac{1}{3}}_{I,j,k} + \\
&+ \frac{\mu_2 H_0 \bar{d}^n_{I,j,k} + 4\Delta x L \bar{c}_{I,j,k}}{\mu_2 H_0 (3\bar{c}_{I,j,k} - \bar{a}_{I,j,k})}
\end{aligned}\right\} \quad (48)$$

Comparing the equalities (46) and (48) the boundary values of $h^{n+\frac{1}{3}}_{I,j,k}$ and $H^{n+\frac{1}{3}}_{I,j,k}$ on the surfaces are:

$$h^{n+\frac{1}{3}}_{I,j,k} =$$

$$= \frac{\mu_0 n_0 h_0 (3c_{I,j,k} - a_{I,j,k})\beta_{I,j,k} - \mu_0 n_0 h_0 d^n_{I,j,k} - 4\Delta x L c_{I,j,k}}{4\mu_0 n_0 h_0 c_{I,j,k} - 4\Delta x L c_{I,j,k} - b_{I,j,k}\mu_0 n_0 h_0 - \mu_0 n_0 h_0 (3c_{I,j,k} - a_{I,j,k})\alpha_{I,j,k}}$$

$$H^{n+\frac{1}{3}}_{I,j,k} = \frac{\mu_2 H_0 (3\bar{c}_{I,j,k} - \bar{a}_{I,j,k})\bar{\beta}_{I,j,k} - \mu_2 H_0 \bar{d}^n_{I,j,k} - 4\Delta x L \bar{c}_{I,j,k}}{4\bar{c}_{I,j,k} - 4\Delta x L - \mu_2 H_0 \bar{b}_{I,j,k} - \mu_2 H_0 (3\bar{c}_{I,j,k} - \bar{a}_{I,j,k})\bar{\alpha}_{I,j,k}}$$

Finally, groundwater levels are computed via the backward sweep method, extended across all layers: $n+1, n+\frac{2}{3}, \ldots$ and so on. After the values are obtained, the convergence of the iterative process is checked based on:

$$\left|(h^{n+\frac{1}{3}}_{i,j,k})^{(s+1)} - (h^{n+\frac{1}{3}}_{i,j,k})^{(s)}\right| < \varepsilon, \left|(H^{n+\frac{1}{3}}_{i,j,k})^{(s+1)} - (H^{n+\frac{1}{3}}_{i,j,k})^{(s)}\right| < \varepsilon,$$

$$\left|(h^{n+\frac{2}{3}}_{i,j,k})^{(s+1)} - (h^{n+\frac{2}{3}}_{i,j,k})^{(s)}\right| < \varepsilon, \left|(H^{n+\frac{2}{3}}_{i,j,k})^{(s+1)} - (H^{n+\frac{2}{3}}_{i,j,k})^{(s)}\right| < \varepsilon,$$

$$\left|(h^{n+1}_{i,j,k})^{(s+1)} - (h^{n+1}_{i,j,k})^{(s)}\right| < \varepsilon, \left|(H^{n+1}_{i,j,k})^{(s+1)} - (H^{n+1}_{i,j,k})^{(s)}\right| < \varepsilon$$

where ε is the accuracy level of the iterative process and s is the order of the iteration.

IV. RESULTS AND DISCUSSION

Simulations were performed to analyze the dynamics of unconfined (upper) and confined (lower) aquifers in a two-layer groundwater system. The proposed three-dimensional mathematical model was implemented in MATLAB R2023a and Python 3.11. The numerical computations employed the finite difference method, with Python libraries, such as NumPy, SciPy, and Matplotlib, used for calculations and visualization. MATLAB was deployed for cross-validation, stability checks, and performance verification of the model.

The computational grid parameters, including spatial steps $\Delta x, \Delta y, \Delta z$, time increment, and convergence criteria, were carefully calibrated to ensure accuracy and numerical stability. At each time step, the system was assembled in matrix form and solved iteratively, providing a spatio-temporal representation of groundwater level variation.

This dual-platform approach, with Python and MATLAB, improved the robustness and reproducibility of the framework. The algorithm followed a structured sequence: grid generation, system assembly, iterative solution, and visualization. The resulting 3D graphs were normalized within the range [0, 1] and reflect the spatial distribution of the levels over time (Table I).

TABLE I. VALUES OBTAINED

μ_1	μ_2	k_1	k_2	n_0	m
0.3	0.2	1×10^{-4}	1×10^{-5}	0.35	10
f	ω	Q	η	t	
1×10^{-3}	5×10^{-5}	1×10^{-3}	0.8	432000	

Utilizing the described numerical algorithm, the spatial and temporal variations in groundwater levels for both unconfined (upper) and confined (lower) aquifers were simulated through a three-dimensional, two-layer differential model. The upper

aquifer (Figure 1) exhibited dome-shaped saturation zones corresponding to recharge areas, while the confined aquifer (Figure 2) displayed a gradual pressure decline, especially near boundaries, consistent with drainage or abstraction.

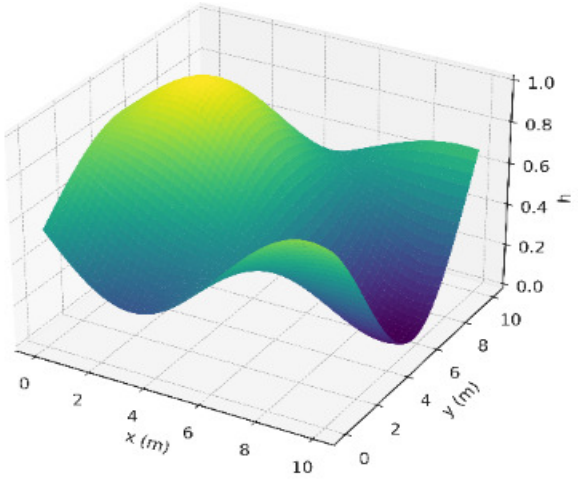

Fig. 1. Variation in the surface water level over time.

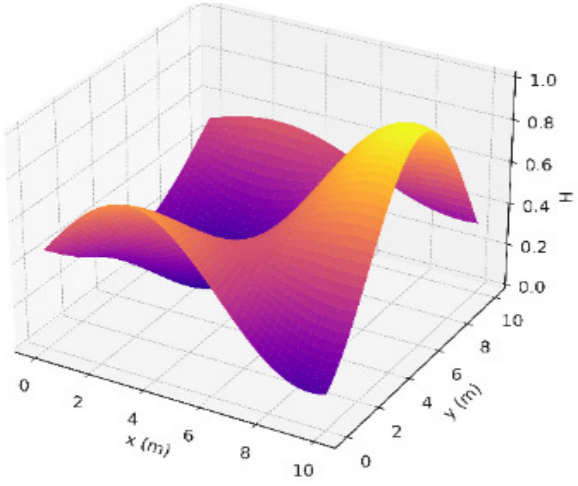

Fig. 2. Variation in the pressure water level over time.

The domed contours of the graph in Figure 1 show the maximum, close to 1, and the minimum, close to 0, values of the water level. In natural conditions, this indicates zones with high filtration rates or saturation due to external influences, such as rainfall or irrigation. The high-intensity changes are caused by factors, such as porosity, evaporation, and external influences.

In the graph in Figure 2, a significant downward trend in the pressure water level is observed, which indicates a decrease in the amount of water in the pressurized layer, caused by an increase in the water extraction rate or by the interaction with the upper layer (filtration flow). In the pressurized layer, a reduction in water pressure is observed from the center toward the outer zones, which may indicate water flow extracted through geophysical fractures or industrial equipment.

To benchmark performance, results were compared with a conventional 2D MODFLOW simulation. This solution underestimated localized pressure changes within ±0.05 units, whereas the proposed 3D model detected variations up to ±0.21 units in fractured zones. This demonstrates the ability of the new model to capture complex vertical leakage and depressurization processes often obscured in lower-dimensional frameworks.

Another presentation of the data in the Table I is the isohyet, contour plots of groundwater levels. In the unconfined aquifer (Figure 3), tightly clustered contours indicate steep gradients and active recharge or filtration zones, while the confined aquifer (Figure 4) displayed broader spacing, consistent with a stable but slowly declining pressure regime.

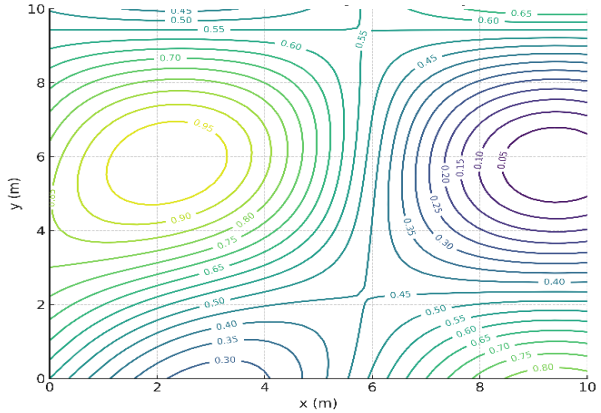

Fig. 3. Contour graph of the variation in the surface water level over time.

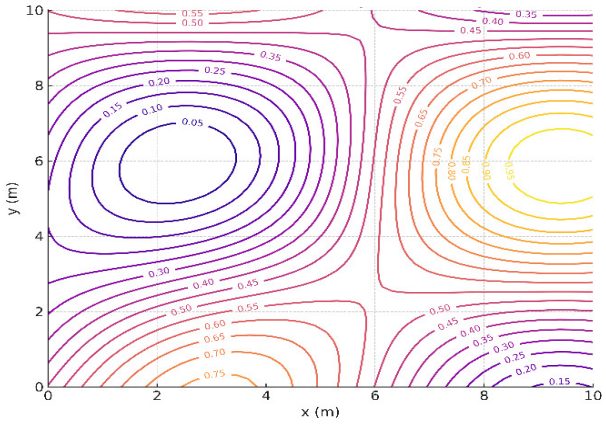

Fig. 4. Contour graph of the variation in the pressure water level over time.

The isohyet analysis of Figure 3 showed that groundwater in the unconfined aquifer was most frequently distributed within the 0.4–0.5 range with 409 points, indicating stable operating levels. Lower values in the range of 0.0–0.3 with 382 points reflected evaporation, low porosity, or slow infiltration, while the intermediate ranges captured gradual declines. In the confined aquifer (Figure 4), pressure levels were also concentrated in the 0.3–0.5 range with 745 points, suggesting stable operating conditions. Lower values in the range of 0.0–

0.1 with 183 points revealed localized depressurization, likely linked to pumping, drainage, or fracture-induced leakage.

The model accuracy was validated against control well data over five simulation days using two widely accepted statistical metrics: Root Mean Square Error (RMSE) and Nash–Sutcliffe Efficiency (NSE) (Table II).

TABLE II. ERROR METRIC VALUES

RMSE	
Unconfined aquifer	0.036
Confined aquifer	0.042
NSE	
Unconfined aquifer	0.81
Confined aquifer	0.77

The dual-layer 3D model advances the hydrogeological analysis by explicitly incorporating porous–fracture flow interactions. Its key features include: the simulation of vertical leakage between hydrostratigraphic units, identification of pressure sink zones caused by abstraction or recharge, and representation of anisotropic flow due to heterogeneous porosity and permeability.

These strengths provide clear practical applications like:

- Water resource management: accurate delineation of recharge zones and optimization of artificial infiltration.
- Risk assessment: early detection of depressurization or overexploitation.
- Infrastructure planning: improved wellfield design with minimized hydraulic interference.
- Environmental monitoring: predictive evaluation of groundwater response to climate and human impacts.

Overall, the 3D two-layer model provides a realistic representation of groundwater dynamics, revealing that the unconfined aquifer is more sensitive to recharge, evaporation, and porosity, while the confined aquifer exhibits slower but sustained pressure declines. The frequent isohyet range of 0.4–0.5 in both layers represents the main operating level of the system. With improved accuracy, structural detail, and interpretability, the model constitutes a robust tool for both scientific research and decision-making in groundwater management.

V. CONCLUSIONS

This study confirms the effectiveness of mathematical and numerical modeling based on differential equations for analyzing hydrodynamic processes in groundwater systems. The proposed two-layer model enabled the simulation of groundwater level variations in both unconfined and confined aquifers, with the results visualized through 3D relief and isoline graphs and validated using statistical indicators.

The modeling framework incorporated key hydrogeological parameters, such as filtration coefficients, porosity, evaporation, external recharge, interlayer permeability, and abstraction rates. The results showed that the unconfined aquifer exhibited significant spatial variability, particularly within the 0.3–0.5 range, where dense contour zones indicated active filtration processes. In contrast, the confined aquifer displayed a gradual but stable decline in pressure head, reflecting a more controlled regime. The analysis also identified irregular flow disruptions arising from the interaction of Newtonian and viscoelastic fluids for which mathematical stabilization conditions were formulated.

The scientific contribution of this work lies in extending geo-filtration modeling, which was traditionally applied to single-layer systems, to a two-layered framework while accounting for both internal and external influences. This enhancement increases the realism and applicability of the model and provides a basis for investigating groundwater salinization dynamics.

From a practical standpoint, the software implementation of the proposed algorithm improves the accuracy in monitoring, forecasting, and assessing groundwater mineralization. It also reduces the need for extensive field experiments by enabling efficient computer-based simulations. Beyond its academic value, this modeling approach offers practical solutions for sustainable water management, including the identification of new freshwater reserves, optimization of groundwater use, design of hydraulic engineering systems, and support for environmental monitoring.

NOMENCLATURE

- $h(x, y, z, t)$, $H(x, y, z, t)$ - are the levels of ground and pressure waters (m)
- μ_1, μ_2 – are the dimensionless coefficients of water loss
- k_1, k_2 – are the filtration coefficients of the upper and lower formations (m/s)
- f – is the external source (%)
- n_0 – is the dimensionless porosity
- ω – is the evaporation (%)
- m – is the thickness of the separating layer (m)
- Q – is the debit (m^3/s)
- η – is the coefficient for converting the model into a dimensional form ($1/m^2$)
- L – is the characteristic length
- $(k_1)_0$, $(k_2)_0$ – are the maximum filtration coefficients
- m_0 – denotes the maximum layer thickness
- Q_0 – represents the maximum discharge

Note: The dimensionless formulation normalizes all variables within [0, 1] to ensure numerical stability when parameters with different units are involved.

REFERENCES

[1] A. Ahmadi *et al.*, "Groundwater Level Modeling with Machine Learning: A Systematic Review and Meta-Analysis," *Water*, vol. 14, no. 6, Jan. 2022, Art. no. 949, https://doi.org/10.3390/w14060949.

[2] A. Mosavi *et al.*, "Susceptibility mapping of groundwater salinity using machine learning models," *Environmental Science and Pollution Research*, vol. 28, no. 9, pp. 10804–10817, Mar. 2021, https://doi.org/10.1007/s11356-020-11319-5.

[3] A. Lal and B. Datta, "Robust Ensemble Modeling Paradigm for Groundwater Salinity Predictions in Complex Aquifer Systems," in *Groundwater Resources Development and Planning in the Semi-Arid Region*, C. B. Pande and K. N. Moharir, Eds. Cham: Springer International Publishing, 2021, pp. 53–72.

[4] S. Alaghmand, S. Beecham, and A. Hassanli, "A review of the numerical modelling of salt mobilization from groundwater-surface water interactions," *Water Resources*, vol. 40, no. 3, pp. 325–341, May 2013, https://doi.org/10.1134/S009780781303010X.

[5] S. Afrifa, T. Zhang, P. Appiahene, and V. Varadarajan, "Mathematical and Machine Learning Models for Groundwater Level Changes: A Systematic Review and Bibliographic Analysis," *Future Internet*, vol. 14, no. 9, Sept. 2022, Art. no. 259, https://doi.org/10.3390/fi14090259.

[6] M. El-Rawy, W. Zijl, A. Salem, A. Awad, M. G. Eltarabily, and A. M. Negm, "Fundamentals of Groundwater Modeling Methods and a Focused Review on the Groundwater Models of the Nile Valley Aquifer," in *Sustainability of Groundwater in the Nile Valley, Egypt*, A. M. Negm and M. El-Rawy, Eds. Cham: Springer International Publishing, 2022, pp. 39–70.

[7] L. Jiao, N. Lu, W. Fang, Z. Li, J. Wang, and Z. Jin, "Determining the independent impact of soil water on forest transpiration: A case study of a black locust plantation in the Loess Plateau, China," *Journal of Hydrology*, vol. 572, pp. 671–681, May 2019, https://doi.org/10.1016/j.jhydrol.2019.03.045.

[8] F. Kazemi, M. Rabbani, and M. Jozay, "Investigating the plant and air-quality performances of an internal green wall system under hydroponic conditions," *Journal of Environmental Management*, vol. 275, Dec. 2020, Art. no. 111230, https://doi.org/10.1016/j.jenvman.2020.111230.

[9] H. I. Chaminé, M. J. Afonso, and M. Barbieri, "Advances in Urban Groundwater and Sustainable Water Resources Management and Planning: Insights for Improved Designs with Nature, Hazards, and Society," *Water*, vol. 14, no. 20, Jan. 2022, Art. no. 3347, https://doi.org/10.3390/w14203347.

[10] R. Meyer, P. Engesgaard, and T. O. Sonnenborg, "Origin and Dynamics of Saltwater Intrusion in a Regional Aquifer: Combining 3-D Saltwater Modeling With Geophysical and Geochemical Data," *Water Resources Research*, vol. 55, no. 3, pp. 1792–1813, 2019, https://doi.org/10.1029/2018WR023624.

[11] C. Qin, Z. Tang, J. Chen, and X. Chen, "The impact of soil and water resource conservation on agricultural production- an analysis of the agricultural production performance in Zhejiang, China," *Agricultural Water Management*, vol. 240, Oct. 2020, Art. no. 106268, https://doi.org/10.1016/j.agwat.2020.106268.

[12] P. Soundala and P. Saraphirom, "Impact of climate change on groundwater recharge and salinity distribution in the Vientiane basin, Lao PDR," *Journal of Water and Climate Change*, vol. 13, no. 11, pp. 3812–3829, Oct. 2022, https://doi.org/10.2166/wcc.2022.161.

[13] N. Li, H. Lyu, G. Xu, G. Chi, and X. Su, "Hydrogeochemical changes during artificial groundwater well recharge," *Science of The Total Environment*, vol. 900, Nov. 2023, Art. no. 165778, https://doi.org/10.1016/j.scitotenv.2023.165778.

[14] A. J. Frankel, "On Per- and Polyfluoroalkyl Substances: Suggested Resources and Considerations for Groundwater Professionals," *Groundwater*, vol. 59, no. 4, pp. 481–487, 2021, https://doi.org/10.1111/gwat.13101.

[15] T. Kim, D. Lee, J. Shin, Y. Kim, and Y. Cha, "Learning hierarchical Bayesian networks to assess the interaction effects of controlling factors on spatiotemporal patterns of fecal pollution in streams," *Science of The Total Environment*, vol. 812, Mar. 2022, Art. no. 152520, https://doi.org/10.1016/j.scitotenv.2021.152520.

[16] M. Ismail, S. M. Pradhanang, T. Boving, S. Motta, B. McCarron, and A. Volk, "Review of Modeling Approaches at the Freshwater and Saltwater interface in Coastal Aquifers," *Land*, vol. 13, no. 8, Aug. 2024, Art. no. 1332, https://doi.org/10.3390/land13081332.

[17] B. Zhang, S. Wang, and Y. Wang, "Probabilistic Projections of Multidimensional Flood Risks at a Convection-Permitting Scale," *Water Resources Research*, vol. 57, no. 1, 2021, Art. no. e2020WR028582, https://doi.org/10.1029/2020WR028582.

[18] L. K. Al-Waeli, J. H. Sahib, and H. A. Abbas, "ANN-based model to predict groundwater salinity: A case study of West Najaf–Kerbala region," *Open Engineering*, vol. 12, no. 1, pp. 120–128, Jan. 2022, https://doi.org/10.1515/eng-2022-0025.

[19] M. H. Msaddek, B. Abdelkarim, L. Zouhri, and Y. Moumni, "Groundwater Salinity Prediction in Deep Desert-Stressed Aquifers Using a Novel Multi-Stage Modeling Framework Integrating Enhanced Ensemble Learning and Hybrid AI Techniques," *Water*, vol. 17, no. 16, Jan. 2025, Art. no. 2452, https://doi.org/10.3390/w17162452.

[20] F. Tian, Y. Zhang, and S. Lu, "Spatial-temporal dynamics of cropland ecosystem water-use efficiency and the responses to agricultural water management in the Shiyang River Basin, northwestern China," *Agricultural Water Management*, vol. 237, July 2020, Art. no. 106176, https://doi.org/10.1016/j.agwat.2020.106176.

[21] L. B. Ball, T. A. Davis, B. J. Minsley, J. M. Gillespie, and M. K. Landon, "Probabilistic Categorical Groundwater Salinity Mapping From Airborne Electromagnetic Data Adjacent to California's Lost Hills and Belridge Oil Fields," *Water Resources Research*, vol. 56, no. 6, 2020, Art. no. e2019WR026273, https://doi.org/10.1029/2019WR026273.

[22] M. Alquraish, "Modeling and Simulation of Manufacturing Processes and Systems: Overview of Tools, Challenges, and Future Opportunities," *Engineering, Technology & Applied Science Research*, vol. 12, no. 6, pp. 9779–9786, Dec. 2022, https://doi.org/10.48084/etasr.5376.

[23] S. Daliev, D. Karshiev, Y. Islamov, and U. Sharipova, "Mathematical modeling of salt concentration change process in two-layer aqueous media," *E3S Web of Conferences*, vol. 401, 2023, Art. no. 02009, https://doi.org/10.1051/e3sconf/202340102009.

[24] S. Daliev, S. Xudoyberdiyev, Z. Abdullayeva, and G. Shikhnazarova, "Three-dimensional mathematical model of groundwater level and salt concentration changes in a single-layer media," *AIP Conference Proceedings*, vol. 3045, no. 1, Mar. 2024, Art. no. 050014, https://doi.org/10.1063/5.0198025.

[25] B. Khuzhayorov, B. Fayziev, O. Sagdullaev, J. Makhmudov, and U. Saydullaev, "A Model of the Degrading Solute Transport in Porous Media based on the Multi-Stage Kinetic Equation," *Engineering, Technology & Applied Science Research*, vol. 15, no. 2, pp. 20919–20926, Apr. 2025, https://doi.org/10.48084/etasr.8986.